mathematics

Article

Multi-Objective Optimization of Cell Voltage Based on a Comprehensive Index Evaluation Model in the Aluminum Electrolysis Process

Chenhua Xu [1,*], Wenjie Zhang [1], Dan Liu [1], Jian Cen [1,2], Jianbin Xiong [1] and Guojuan Luo [1]

[1] School of Automation, Guangdong Polytechnic Normal University, Guangzhou 510665, China
[2] Guangzhou Intelligent Building Equipment Information Integration and Control Key Laboratory, Guangzhou 510665, China
* Correspondence: xchhelen@163.com

Abstract: In the abnormal situation of an aluminum electrolysis cell, the setting of cell voltage is mainly based on manual experience. To obtain a smaller cell voltage and optimize the operating parameters, a multi-objective optimization method for cell voltage based on a comprehensive index evaluation model is proposed. Firstly, a comprehensive judgment model of the cell state based on the energy balance, material balance, and stability of the aluminum electrolysis process is established. Secondly, a fuzzy neural network (FNN) based on the autoregressive moving average (ARMA) model is designed to establish the cell-state prediction model in order to finish the real-time monitoring of the process. Thirdly, the optimization goal of the process is summarized as having been met when the difference between the average cell voltage and the target value reaches the minimum, and the condition of the cell is excellent. And then, the optimization setting model of cell voltage is established under the constraints of the production and operation requirements. Finally, a multi-objective antlion optimization algorithm (MOALO) is used to solve the above model and find a group of optimized values of the electrolysis cell, which is used to realize the optimization control of the cell state. By using actual production data, the above method is validated to be effective. Moreover, optimized operating parameters are used to verify the prediction model of cell voltage, and the cell state is just excellent. The method is also applied to realize the optimization control of the process. It is of guiding significance for stabilizing the electrolytic aluminum production and achieving energy saving and consumption reduction.

Keywords: cell voltage; multiple targets; optimal control; electrolytic aluminum; aluminum electrolytic cell

MSC: 93C10

check for updates

Citation: Xu, C.; Zhang, W.; Liu, D.; Cen, J.; Xiong, J.; Luo, G. Multi-Objective Optimization of Cell Voltage Based on a Comprehensive Index Evaluation Model in the Aluminum Electrolysis Process. *Mathematics* **2024**, *12*, 1174. https://doi.org/10.3390/math12081174

Academic Editors: Zhi Li and Sihai Guan

Received: 11 March 2024
Revised: 5 April 2024
Accepted: 9 April 2024
Published: 14 April 2024

1. Introduction

The aluminum electrolytic production process mainly uses cryolite-alumina as a raw material, carbon as the anode and cathode of the electrolytic reaction, and is carried out by passing a strong direct current into the electrolytic cell to induce the electrochemical reaction in the cell, so as to complete the electrolytic aluminum production [1]. In actual production, costs play an important role to affect the development of capacity. And the cost of the largest proportion is the price of electricity, which varies and accounts for about 30% to 35% of the cost in different regions [2]. At present, with the decreasing resources of the Earth and the rising price of electricity, the cost of aluminum electrolysis production is getting higher and higher. Thus, it is important to achieve energy-saving and consumption reduction in the production of aluminum electrolysis. The method of energy saving in aluminum electrolysis is generally by improving current efficiency and reducing cell voltage [3]. Due to the complexity of improving current efficiency, most companies nowadays reduce the cell voltage to save energy and decrease consumption. However, the optimal cell voltage cannot be found by manually adjusting and changing a single parameter.

Cell voltage refers to the voltage through which the current passes in the electrolytic cell, and it is an important factor in the production process of aluminum electrolysis [4]. The parameters affecting cell voltage are the pole pitch, electrolyte level, molecular ratio, resistance, alumina concentration, aluminum output, electrolyte temperature, aluminum level, and electric current. All these parameters change in real time with cell state and cannot be measured online in real time [5]. DC power consumption is the most important part of production energy consumption, which is directly proportional to the size of the cell voltage, so appropriately reducing the cell voltage is one of the methods to achieve energy saving and consumption reduction in aluminum electrolysis [6]. At present, aluminum electrolysis production mainly relies on manual experience to control. However, due to the nonlinear and strong coupling relationship between aluminum electrolysis production parameters, to achieve the purpose of reducing consumption and increasing production, the manual adjustment of certain parameters may lead to the transformation of the state of the aluminum electrolysis cell to the evil cell. It is necessary to appropriately reduce the voltage of the electrolytic cell, and then use the corresponding method to optimally control the state of the electrolytic cell to produce electrolytic aluminum under the best conditions, conducive to energy-saving and consumption-reducing production.

Aluminum electrolysis data are characterized by strong coupling and nonlinearity, making it difficult to obtain to establish the relationship between sampled parameters and the cell state. To address this challenge of whether the cell state judgment is accurate or not. Researchers have predicted the aluminum electrolysis cell state by the methods of mechanism modeling, machine learning, and deep learning. Cui et al. proposed a method combined the multi-support vector machine with the cell condition classification based on fuzzy C-mean algorithm to predict aluminum electrolysis concentration, so as to judge the state of the cell [7]. He et al. proposed the use of deep learning to determine whether the aluminum electrolysis process would have an anodic effect, and thus whether the cell state would be in a normal or abnormal state [8]. Gao et al. used a neural network algorithm to predict the state of aluminum electrolysis cells [9]. Hou et al. proposed an LSTM-based prediction of aluminum electrolysis cell conditions [10]. Xu et al. proposed a multiple limit learning machine based on a genetic algorithm to realize the prediction of cell voltage [11]. However, due to the interference of external environment, the prediction effect often cannot reach the ideal state. Therefore, some other scholars have considered the use of different indicators such as current efficiency, temperature, anode effect, etc., to judge the state of aluminum electrolysis cell. Li et al. used the temperature as the main variable to determine whether the thermal equilibrium of the cell is in the normal state by thermocouple thermometry, infrared thermometry, and fiber grating thermometry [12]. Fan et al. achieved the optimization of reducing DC energy consumption by improving the current efficiency [13]. Some researchers have optimized cell voltage of aluminum electrolysis by using an intelligent algorithm to achieve energy-saving and consumption-reducing production [14,15]. Zhou et al. proposed an improved temporal convolutional network method to classify current sequences for the identification of cell states [16]. However, most of the above methods for optimizing and controlling aluminum electrolysis production are aimed at controlling a single parameter of the electrolytic cell, without judging the cell state from a global perspective. In order to obtain a more accurate cell state, more indicators need to be considered to reflect the production and operation state of the electrolytic cell.

In the actual production process, in order to reduce the industrial energy consumption, enterprises and researchers mostly adopt the strategy of reducing the cell voltage. However, the relationship between the cell voltage and the relevant technical conditions cannot be simply modeled using mathematical expressions [17]. Multi-index modeling can comprehensively consider multiple indicators or factors, making the model more comprehensive and closer to the actual situation. By considering multiple aspects, the complexity of the system can be better understood [18,19]. The relationship between the cell state and technical conditions can be well described by establishing a comprehensive evaluation index of groove state with multiple indexes. Compared with the traditional FCM algorithm, the adaptive FCM algorithm has stronger robustness, faster convergence speed, and wider applicability [20,21]. Therefore, the use of a multi-index comprehensive judgment model combined with an adaptive FCM algorithm can better judge the status of electrolytic cell. At present, the ARMA model is widely used in time-series data modeling and prediction for its advantages of wide applicability, simple use, and strong model interpretability. Gao et al. used the ARMA algorithm to analyze the historical data of abnormal population aggregation to predict the trend of abnormal human aggregation [22]. Sansa et al. established the ARMA model for small changes in solar radiation and predicted the changes in solar radiation more accurately [23]. The FNN algorithm has the advantages of strong adaptability, high parallel computing efficiency, strong generalization ability, flexible processing function approximation, and prediction problems [24]. Therefore, the ARMA-FNN prediction model is established to monitor the state of the prediction cell in real time. In addition, the establishment of relevant models according to the process itself can not only optimize the process parameters, but also optimize the model through continuous collection of analysis data [6]. In the aspect of cell voltage setting, the multi-objective optimization model of cell voltage can be established with the minimum difference between the average voltage and the target value and the good state of the cell as the goal, and the production operation requirement as the constraint condition, so as to obtain a set of better operating parameters, so as to achieve the purpose of energy saving and consumption reduction.

In this paper, when the cell condition is transformed into a wicked cell, a multi-objective optimization method of the cell voltage of the aluminum electrolysis process based on the comprehensive index judging model is proposed. First, a comprehensive index of cell states is established, and the cell states are categorized by the fuzzy C-means (FCM) clustering algorithm. Then, because of the severe hysteresis characteristics of the electrolysis cell, a cell-state model based on a fuzzy neural network is established to predict the trend of the cell state in the next 24 h. Finally, the important parameters of cell voltage are analyzed and simplified by using the PP algorithm. Aiming at the strong coupling characteristics between the parameters of aluminum electrolysis, the optimization setting model of the operating parameters is established to provide guidance for the energy-saving production of aluminum electrolysis.

2. Comprehensive Evaluation Model of Cell State

2.1. Mechanism Analysis

Aluminum electrolysis is a production process accompanied by many complex physical and chemical changes. There are many parameters to affect the cell state in the process, so that the cell state of aluminum electrolysis has complex and variable characteristics. A change in raw materials and operating parameters will probably transform a cell in good condition into a cold cell, hot cell, sick cell, or other bad cell.

The operating state of an electrolytic cell includes thermal balance state, material balance state, and stability state. The thermal equilibrium state of an electrolysis cell is defined as the state under the externally supplied electrical energy equaling the energy consumed by the decomposition of the alumina; that is, the heat income equals the heat expenditure. When the thermal equilibrium is disturbed, it will cause abnormal fluctuations in the electrolyte temperature. Material equilibrium is defined as a balanced relationship between the raw materials fed into the electrolysis cell and the raw materials consumed by the electrolysis process. The electrolyte height and the excess of aluminum fluoride can reflect the amount of material input, and the aluminum level and the amount of aluminum output reflect the amount of material consumption. If the amount of input is not equal to the amount of consumption, it will lead to fluctuations in the molecular ratio and the concentration of alumina in the electrolytic cell so as to cause the anode effect. Noise from the anode effect is a main parameter reflecting the stability of the electrolytic cell. In summary, aluminum fluoride excess (x_1), electrolyte temperature (x_2), aluminum level (x_3), aluminum output (x_4), alumina concentration (x_5), molecular ratio (x_6), noise (x_7), and electrolyte height (x_8) can be used as parameters to classify cell states.

DC power consumption is the most important part of production energy consumption. The relationship of cell voltage and current efficiency is defined as follows [25].

$$\text{DC power consumption} = \frac{2980 \times \text{average voltage}}{\text{Current efficiency}} \tag{1}$$

In the production process, the cell state is evaluated according to the experiences. The smaller the DC power consumption of the process is, the better the corresponding cell state is. That is, the average cell voltage is as small as possible, while the current efficiency is as large as possible. In addition, the anode effect reflects the stability of the electrolytic cell. The shorter the cumulative duration of the anode effect is, the better the cell condition is. Therefore, the degree of deviation of three parameters including the average cell voltage, current efficiency, and cumulative duration of anode effect from the ideal situation can be used as a comprehensive index for evaluating the state of an electrolytic cell.

2.2. Comprehensive Index of Cell State

After the state of an electrolytic cell is analyzed, the difference between its parameters in the equilibrium state and those in the ideal state is evaluated. These parameters contain cumulative effect time (T), average cell voltage (V), and current efficiency (W). The extent to the values of the three parameters deviating from the ideal conditions in the cell can be used as a basis for judging the cell state. In order to finish the optimization and control of the cell state, the cumulative incidence of anodic effects in a day is hoped to be less, the average cell voltage close to the optimized value, and the current efficiency achieving to 1. Therefore, the comprehensive cell state space is shown in Equation (2).

$$(u, v, w) = (\frac{T}{24}, \frac{V - V_{\text{sup}}}{V_{\text{sup}}}, 1 - W) \tag{2}$$

where V_{sup} is the optimized cell voltage. The u, v, and w represents the degree of deviation of the three quantities T, V, and W from the ideal state. A group of different (u, v, w) can represent a different cell state. The distance between (u, v, w) and the coordinate point of origin is used to measure the degree of superiority of the cell state.

Therefore, the composite index of cell state is defined as follows.

$$d = \sqrt{u^2 + v^2 + w^2} \tag{3}$$

where d is the distance between (u, v, w) and the point of origin. It means that the larger d is, the greater the corresponding cell state of the sample point deviates from the ideal state, and the worse the cell state is. On the contrary, the cell state is better.

2.3. Comprehensive Judgment Model Based on FCM Cell State

In the process of cell state assessment, it is necessary to cluster similar cell states together. It is called clustering analysis of electrolytic cell states. Fuzzy cluster analysis is a mathematical method of classification using fuzzy mathematical language. Aiming at the fuzzy characteristics of the cell state, the adaptive FCM algorithm is adopted to determine the affinity degree of the samples to realize the electrolytic cell state classification. The superiority of the proposed algorithm is that the number of clustering categories C of adaptive FCM takes values according to different experimental samples compared with traditional FCM. The affiliation matrix is defined as follows.

$$U = \{u_{ij} \big| i = 1 : n, j = 1 : C\} \tag{4}$$

where the samples of it are obtained for each experiment, and u_{ij} represents the affiliation of the i-th sample for the j-th class. The variable I explains the correlation of the i-th sample to the j-th class and is defined in the following equation.

$$I = \max(u_{ij}) \tag{5}$$

where the larger I is, the higher the correlation that the sample is assigned to that class. The samples set of cell state is set for $\{x(i,j)|i = 1:n, j = 1:p\}$.

The implementation steps of the adaptive FCM algorithm are as follows.

Step 1: Determine the number of cell state categories C, n is the number of samples, V_0 is the original clustering center, and set the initial iteration number t equal to 0.

Step 2: Calculate the cell state category classification matrix U of the sample according to Equation (6).

$$u_{ij} = [\sum_{k=1}^{C} (\frac{\|x_i - v_j\|^2}{\|x_i - v_k\|^2})^{\frac{1}{m-1}}]^{-1}, 1 \le i \le n, 1 \le j \le C \tag{6}$$

where x_i is the i-th sample, v_j is the j-th center of clustering, v_k is the k-th center of clustering, and u_{ij} is the degree of affiliation of x_i to v_j. m is equal to 2.

Step 3: Calculate the clustering center for the next iteration $V(t+1)$ according to Equation (7).

$$v_j = \frac{\sum_{i=1}^{N} (u_{ij})^m x_i}{\sum_{i=1}^{N} (u_{ij})^m}, 1 \le j \le C \tag{7}$$

where v_j is the current clustering center.

Step 4: If

$$\|V(t) - V(t+1)\| \le \varepsilon \tag{8}$$

is true, then output the category partition matrix and the clustering center V. Otherwise, go to Step 1, where ε is the iteration stopping threshold.

Step 5: If $\overline{I}$ is maximal, stop. Otherwise, go to Step 1.

Step 6: The degree of deviation of the three quantities T, V, and W from the ideal state, that is (u, v, w), is derived from Equation (2).

Step 7: According to Equation (3), the composite index of cell state d is calculated for each category, with the larger d being assessed as a poor cell, and the smaller d being assessed as an excellent cell.

3. Cell-State Prediction Model Based on ARMA-FNN

When the electrolytic cell is disturbed and transited into a bad cell, the settings of controllable parameters can be adjusted in time according to the current state to prevent the electrolytic cell state from turning in a worse cell. To correctly predict the electrolytic cell state is the key to preventing the cell from transforming into a bad result. Therefore, a model for predicting the cell state is developed. As analyzed in Chapter 1, the variable d can reflect the production status of the electrolytic cell from a global perspective. Moreover, when the inputs of control system are unchanged, the variable d will evolve in a stable trend. When the inputs of control system are changed, the variable d will change with the original because a worker modifies the setting of controllable parameter in response to a change in cell state. Thus, the future cell state contains two parts. One is the historical continuation d_{k+1} of the current state d_k, and the other is the control effect of the current input of the system. To predict the future cell state, the composite index d is predicted by using a time-series method, and then a neural network is used to fuse d_{k+1} with the input parameters of the system.

3.1. Comprehensive Cell Condition Indicator Time-Series Prediction Model Based on ARMA

The time series of the comprehensive index d is similar to being stable. In a word, if the inputs to the system are constant, d will evolve in a relatively stable trend. The ARMA model is one of most widely used methods in time series. It firstly makes a difference operation to change the original series into a smooth time series. Then, an auto-correlation function (ACF) and partial auto-correlation function (PACF) are used to determine the initial order. Finally, the above function is estimated by the maximum likelihood method or weighted least squares method. The ARMA (m, n) model consists of an auto-regressive (AR) and moving average (MA). The general representation of the model is described in Equation (9) [26].

$$x_t = \varphi_1 x_{t-1} + \varphi_2 x_{t-2} + \cdots + \varphi_n x_{t-n} - \theta_1 a_{t-1} - \theta_2 a_{t-2} - \cdots - -\theta_m a_{t-m} + a_t \tag{9}$$

where x_t is the cell-state indicator d observed at moment t. $\varphi_i (1 \leq i \leq n)$ is the auto-regressive coefficient, $\theta_j (1 \leq j \leq n)$ is the moving average coefficient, and a_t is the white noise sequence.

The m and n in an ARMA model are generally determined by the Akaike information criterion (AIC) [27–29]. If the AIC of the ARMA (m, n) is minimized, then it means that the model is the most effective in forecasting the time series. The AIC criterion is shown in Equation (10).

$$AIC(l) = \widehat{\log \sigma_a^2} + \frac{2l}{N} \tag{10}$$

where $l = m + n$, σ_a^2 denotes the error variance of the model and N is the number of observations.

Because there is complex noise in the time series of the cell state, the AIC can easily fall into the local optimum. The ALO algorithm [30] is adopted to determine the order ARMA (m, n) of the model, and to predict the indicator d of the cell state in the time series. The steps of the algorithm are described. An individual $z = (z_1, z_2)$ represents a set of parameters of ARMA, and the fitness of the individual measures the performance of the algorithm for that set of parameters.

Step 1: Population random initialization. Randomly generate n ants and m antlions, set the upper and lower bounds of the search space U_d and L_d, set the population size N of antlions and ants, and set the maximum number T of iterations.

Step 2: Individual fitness values are calculated according to Equation (11).

$$f(i) = \min[\frac{\sum_{i=1}^{N} (d(i) - \hat{d}(i))^2}{\sum_{i=1}^{N} (d(i) - \overline{d})^2}] \tag{11}$$

where $f(i)$ represents the fitness value of the i-th individual, $\hat{d}(i)$ represents the predicted value of the i-th individual, and $\overline{d}$ represents the mean value of all samples.

Step 3: Update the location of ants, antlions, and elite antlions according to the ALO algorithm.

Step 4: Determine whether the termination condition is satisfied, if not then go to Step 3, if satisfied then obtain the optimization parameter (m, n) and execute the next step.

Step 5: The ARMA (m, n) model is applied to predict d_{k+1}.

3.2. A Prediction Model for Cell State Based on FNN

In the process of aluminum electrolytic production, the state of the electrolytic cell is affected by the workers adjusting the amount of aluminum discharged (x_4). The controllable parameters of electrolytic cell include alumina concentration (x_5), molecular ratio (x_6), and cell resistance (x_9). To obtain the future cell state, the method of fuzzy neural networks is modeled to predict and measure the cell state after controlled parameters happen to change. The inputs of the prediction model is the result of combining d_{k+1} with x_4, x_5, x_6, and x_9. The output of the prediction model is the future cell state (y). The y is defined in the following equation.

$$y = f(d_{k+1}, x_4, x_5, x_6, x_9) \tag{12}$$

The FNN method combines the excellent learning obtained using the computation ability of a neural network with the excellent fuzzy knowledge expression ability of fuzzy theory. Thus, this algorithm is often used in fault diagnosis of production and good diagnostic results are obtained [31]. FNN is used to model the future cell state, and its model structure is shown in Figure 1.

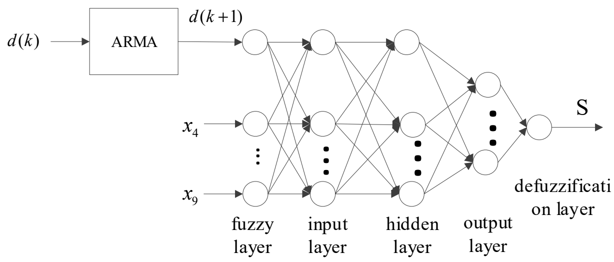

Figure 1. Structure of cell-state prediction model based on FNN.

Considering the single-peak characteristic of cell state, a Gaussian affiliation function is used in the fuzzification layer when modeling cell state. The Gaussian affiliation function is defined as follows.

$$U(x) = e^{-\frac{(x-c)^2}{2\sigma^2}} \tag{13}$$

where the parameter c represents the horizontal coordinate of the peak of the Gaussian affiliation function and the parameter σ represents the standard deviation.

The structure of the prediction model is based on a BP neural network. It has the advantage of setting the number of intermediate layers and the number of neurons in each layer according to the training effect of the model. The model has a good learning ability in dealing with nonlinear problems. The number of neurons in the fuzzification layer is the number of input parameters, equal to 5. The number of neurons in the defuzzification layer is 1. The number of neurons in the input layer is the result of the number of the output parameters multiplying the number of the fuzzification layer equal to 5. The number of neurons in the hidden layer is determined by the following empirical formula.

$$\rho = \sqrt{n+m} + d \tag{14}$$

where ρ is the number of neurons in the hidden layer, n is the number of input parameters, and m is the number of output parameters. $d \in [0, 10]$. Here, ρ is equal to 12.

4. Optimization Setting Model

For the excellent cell state, the operator can adjust the parameters to realize energy-saving production by reducing the cell voltage under the condition of ensuring a good cell state. When the electrolytic cell develops into an evil cell, the controllable parameter settings should be adjusted in time according to the current state to avoid the cell state from turning into a worse cell. For this reason, based on the above result of predicting the cell state in the Section 3.2, an optimized setting model is established according to the control target of adjusted parameters and the requirements of actual operation, and solved by the MOALO algorithm.

4.1. Influencing Cell Voltage Parameters

In electrolytic aluminum production, the electrolyte temperature, alumina concentration, and mole ratio are the main production parameters reflecting the equilibrium of the cell state. When the three parameters change, the conductivity of the electrolyte will be disturbed, so as to change the resistance of the electrolytic cell. If the production current remains constant, the cell voltage changes. The stability of alumina concentration is the key factor to ensure the stability of electrolytic production. When the alumina concentration is too low, anodic effects will happen; at the same time, the cell voltage will rise sharply. Pole pitch is defined as the distance from the bottom palm of the anode to the mirror surface of the aluminum liquid. When pole pitch transits, the resistance between the two poles will change, so as to affect the electrolyte pressure drop and ultimately lead to the change in the cell voltage. Changing the pole pitch is a more accurate and quicker way to change the cell voltage. Therefore, the main method used in the production process is to adjust the cell voltage by adjusting the pole pitch. Aluminum is a good heat conductor, so the height of the aluminum liquid affects the temperature and the heat balance of the electrolytic cell and the stability of the cell voltage.

The electrolyte level relates to the stability of the electrolytic cell. If the electrolyte level is too low, the anode effect occurs when the anode is not sufficiently wetted, which will lead to a high cell voltage. In summary, the main technical conditions affecting the cell voltage (y) were determined by electrolyte temperature (x_2), aluminum level (x_3), aluminum output (x_4), alumina concentration (x_5), molecular ratio (x_6), cell resistance (x_9), pole pitch (x_{10}), electrolyte level (x_{11}), and electric current (x_{12}).

4.2. Data Preprocessing Based on PP Algorithm

The actual production data contain a large amount of information, and there are numerous and only non-linear parameters affecting the cell voltage. In order to accurately analyze the parameters affecting the cell voltage to improve the accuracy of cell voltage prediction, the projection pursuit algorithm (PP) is used for data preprocessing [32]. The correlation of electrolyte temperature (x_2), aluminum level (x_3), aluminum output (x_4), alumina concentration (x_5), molecular ratio (x_6), cell resistance (x_9), pole pitch (x_{10}), electrolyte level (x_{11}), and electric current (x_{12}) to cell voltage are obtained by finding the optimal projection direction in the PP algorithm. The projection function in the PP algorithm is used to optimize the model, and the optimal projection direction can be found by a genetic algorithm to be (0.347, 0.089, 0.196, 0.550, 0.284, 0.628, 0.211, 0.083, 0.189). This is the value of the contribution of these parameters to the cell voltage. Since the contributions of x_3 and x_{11} are significantly smaller than those of x_2, x_4, x_5, x_6, x_9, x_{10}, and x_{12}, the input parameters of the model can be chosen as the electrolyte temperature x_2, the aluminum output x_4, the concentration of alumina x_5, the molecular ratio x_6, the cell resistance x_9, the pole pitch x_{10}, and the electric current x_{12}.

4.3. Model for Optimized Setting of Operating Parameters

In the process of electrolyte use, an electrolytic cell deviating from the optimal production state can be brought back to the optimal state through adjusting these operation parameters including temperature (x_2), aluminum output (x_4), alumina concentration (x_5), molecular ratio (x_6), cell resistance (x_9), pole pitch (x_{10}), and electric current (x_{12}). It is very important for energy saving to keep the fluctuation of cell voltage stable. Therefore, the cell state needs to be restored to the normal and cell fluctuation needs to be kept in stable range. Considering the production operation requirements as the constraints, the optimization setting model is established as follows.

$$fitness_1 = \min[f(\cdot) - V_{\mathrm{sup}}] \tag{15}$$

$$fitness_2 = \min[S(\cdot) - 0] \tag{16}$$

$$\begin{cases} 172 \leq x_2 \leq 174 \\ 0 \leq x_4 \leq 40 \\ M_{base} - 1.3 \leq x_5 \leq M_{base} + 1.3 \\ O_{base} - 0.9 \leq x_6 \leq O_{base} + 0.9 \\ R_{base} - 0.002 \leq x_9 \leq R_{base} + 0.002 \\ 3.9 \leq x_{10} \leq 4.5 \\ 935 \leq x_{12} \leq 965 \end{cases} \tag{17}$$

where R_{base}, O_{base}, and M_{base} obtained by process analysis are the baseline cell resistance, baseline molecular ratio, and baseline alumina concentration, respectively. Here, R_{base} is equal to 0.0113, O_{base} is equal to 2.10, and M_{base} is equal to 3.32.

V_{sup} is obtained by Equation (2) and equal to 3.8446 in this paper [10]. $f(\cdot)$ is the average cell voltage from data collected at the factory, $S(\cdot)$ is the cell-state prediction model from Equation (12), and $\min[S(\cdot) - 0]$ represents the future cell state infinitely close to the optimal cell state. This optimization problem is that the value of the operating parameter needs to be adjusted to meet the requirements through effective intelligent optimization algorithm to restore the cell status to normal.

4.4. Optimization of Operating Parameters Based on MOALO

When solving multi-objective optimization problems, multiple objectives often conflict. As a multi-objective optimization set, Pareto optimal solutions [33,34] are often used to address the best trade-off between objectives.

The MOALO algorithm shows better convergence, accuracy, and robustness on solving multi-objective optimization problems. To search for a highly diverse set of Pareto-optimal solutions, the algorithm uses leader selection and archive maintenance to store Pareto-optimal solutions and roulette rules to select non-dominated solutions from them. The probability of choosing an antlion among them is as follows.

$$P_j = \frac{c}{N_j}, c > 1 \tag{18}$$

where N_j denotes the number of solutions in the neighborhood of the j-th solution and c denotes a constant. If the archive storing the optimal solution is full, the archived solution set will be deleted with the probability of $\frac{1}{P_j}$. Unlike ALO, the antlion position is updated in MOALO, and is described as follows.

$$Antlion_j^k = Ant_i^k, if\ f(Ant_i^k) < f(Antlion_j^k) \tag{19}$$

where $f(Ant_i^k)$ less than $f(Antlion_j^k)$ means that Ant_i^k prevails over $Antlion_j^k$.

The optimization setting model is solved using MOALO as follows.

Step 1: Population random initialization. Randomly generate n ants and m antlions, set the upper and lower bounds of the search space U_d and L_d, set the population size N of antlions and ants, and set the maximum number T of iterations.

Step 2: Calculate individual fitness values.

$$\begin{cases} fitness_1 = \min[f(\cdot) - V_{\text{sup}}] \\ fitness_2 = \min[S(\cdot) - 0] \end{cases} \tag{20}$$

Step 3: Update and archive locations of ants, antlions, and elite antlions according to the ALO algorithm. If the updated ant position is better than the selected antlion, the position of the antlion updates to the ant position.

Step 4: If the archive space is full, a portion of the solution is removed with the probability of $1/P_j$ using a roulette rule.

Step 5: Determine whether the stopping condition is reached. If it is reached, then the algorithm ends and the optimal operation parameter s^* is obtained. Otherwise, jump to Step 3.

To check whether the obtained operating parameters are optimal, the obtained values of the optimized setting are substituted into the cell-state prediction model to be verified. The optimization target is judged by analyzing the value composite index *d*. Furthermore, the derived optimization setpoints can be used to realize optimization control of the process.

5. Experimental Results and Analysis

All the experiments were carried out on MATLAB 2020a platform, and the experimental data were obtained from a factory site.

5.1. Results of Cell-State Evaluation Based on FCM

We took 150 samples for the experiment and set the parameters of the FCM cell state clustering model as follows. The fuzzy weighting index m is equal to 2, the maximum number of iterations is set to 20, and the iteration stopping threshold ε is equal to 10^{-6}. Experiments on FCM-based classification of cell state were carried out when C took different values, and the corresponding $\overline{I}$ values were calculated, and the results are shown in Table 1. From the table, it can be seen that $\overline{I}$ is at a maximum when C is equal to 3, so the parameter C being equal to 3 is used in the cell-state classification model. The results of the clustering experiments are shown in Table 2. The algorithm categorizes 150 sets of samples into 3 classes.

Table 1. The $\overline{I}$ of different *C*.

C	2	3	4	5	6	7	...
I	0.921	0.967	0.845	0.844	0.777	0.761	...

Table 2. Results of clustering.

Categories	Number of Samples/Size
Class1	9
Class 2	31
Class 3	110

The composite index *d* and its range were calculated individually for each type of sample as shown in Table 3. Since the *d* in Class 3 was the lowest, Class 3 was rated excellent and Class 2 was rated good. The *d* in Class 1 was the highest, so Class 1 was rated poor. In this paper, the 150 group samples were experimented on to cluster and evaluate the cell states. The results show that 110 groups remained excellent, 31 groups were good, and 9 groups were poor.

Table 3. Cell-state evaluation results based on adaptive FCM.

Categories	Index *d*	Result
Class 1	0.0758~0.6550	Poor
Class 2	0.0089~0.0545	Good
Class 3	0.0003~0.0086	Excellent

In the same way, current efficiency and apparent cell resistance were used as indicators to evaluate the cell state. Indicators and their ranges were calculated for each of the three categories of sample points and the results are shown in Table 4.

Table 4. Cell-state evaluation based on different indexes.

Categories	Range of Indexes			Result
	Index d	Current Efficiency/%	Cell Resistance/μΩ	
Class 1	0.0758~0.6550	72~85	14.0~16.1	Poor
Class 2	0.0089~0.0545	87~95	13.5~13.9	Good
Class 3	0.0003~0.0086	94~98	13.1~13.6	Excellent

Finally, the above model for judging cell state was validated using 31 additional data, and the results of the validation are shown in Table 4. It is worth noting that if the indicator value of sample is outside the known range in Table 4, it will be assessed as the closest category to it. It can be seen from Table 5 that the probability of correctly evaluating the cell state based on the comprehensive index model reaches 96.78%. It indicates that the proposed method can accurately be used to categorize and evaluate the current cell state. In addition, the experimental results of different assessment index in Table 5 shows that the composite metric d is more advantageous in improving the accuracy of the cell-state evaluation.

Table 5. Evaluation accuracy on different index.

Cell Status Index	Correct Rate/%
Current efficiency	77.42
Cell Resistance	93.55
d	96.78

5.2. Results of Cell-State Prediction Based on FNN

To illustrate the superiority of the ALO algorithm, experiments were conducted with the ALO and PSO and FWA algorithms, respectively, based on the same experimental samples. Firstly, the three algorithms are compared by using a public data set [35]. The population number was set to 30, the dimension was set to 30, and the three algorithms were iterated 1000 times, respectively. The average values and standard deviations of the three algorithms are shown in Table 6 (the bold font indicates the optimal). Secondly, optimization of cell voltage is carried out 10 times, the convergence speed of the three algorithms is shown in Figure 2, and the optimized cell voltage values are shown in Figure 3, respectively. The results of the 10-times optimization are statistically analyzed, and the standard deviation and mean comparison results are shown in Table 7.

Table 6. Comparison of baseline functions. (The bold font indicates the optimal).

Function	FWA		PSO		ALO	
	Mean	Std	Mean	Std	Mean	Std
F_1	1.19×10^{0}	8.15×10^{-1}	4.66×10^{-8}	1.19×10^{-7}	$\mathbf{3.16 \times 10^{-9}}$	$\mathbf{2.56 \times 10^{-9}}$
F_2	6.17×10^{1}	7.22×10^{1}	$\mathbf{9.73 \times 10^{-4}}$	$\mathbf{1.58 \times 10^{-3}}$	1.88×10^{0}	7.42×10^{-1}
F_3	1.18×10^{5}	2.49×10^{4}	1.49×10^{1}	6.75×10^{0}	$\mathbf{1.35 \times 10^{-6}}$	$\mathbf{1.20 \times 10^{-6}}$
F_4	7.88×10^{1}	8.30×10^{0}	6.29×10^{-1}	1.88×10^{-1}	$\mathbf{5.61 \times 10^{-5}}$	$\mathbf{7.89 \times 10^{-5}}$
F_5	4.98×10^{4}	4.45×10^{4}	4.69×10^{1}	2.77×10^{1}	$\mathbf{7.65 \times 10^{0}}$	$\mathbf{1.11 \times 10^{1}}$
F_6	1.04×10^{0}	4.80×10^{-1}	1.39×10^{-8}	3.73×10^{-8}	$\mathbf{2.15 \times 10^{-9}}$	$\mathbf{3.54 \times 10^{-9}}$
F_7	2.03×10^{-2}	7.17×10^{-2}	6.76×10^{-2}	$\mathbf{2.03 \times 10^{-2}}$	$\mathbf{1.32 \times 10^{-2}}$	$\mathbf{2.03 \times 10^{-2}}$
F_8	-6.02×10^{14}	1.84×10^{14}	-5.60×10^{3}	$\mathbf{1.17 \times 10^{2}}$	$\mathbf{-3.10 \times 10^{3}}$	1.34×10^{3}
F_9	2.53×10^{2}	4.58×10^{1}	4.58×10^{1}	$\mathbf{5.15 \times 10^{0}}$	$\mathbf{1.89 \times 10^{1}}$	5.42×10^{0}
F_{10}	6.85×10^{-1}	3.05×10^{-1}	4.38×10^{-5}	6.54×10^{-5}	$\mathbf{2.77 \times 10^{-5}}$	$\mathbf{3.66 \times 10^{-5}}$
F_{11}	9.36×10^{-1}	4.79×10^{-2}	$\mathbf{5.17 \times 10^{-3}}$	$\mathbf{7.38 \times 10^{-3}}$	1.82×10^{-1}	8.92×10^{-2}
F_{12}	2.77×10^{1}	2.91×10^{1}	$\mathbf{3.54 \times 10^{-9}}$	$\mathbf{1.09 \times 10^{-9}}$	9.60×10^{-5}	1.23×10^{-6}
F_{13}	3.57×10^{5}	9.25×10^{5}	2.20×10^{-3}	4.63×10^{-2}	$\mathbf{2.29 \times 10^{-10}}$	$\mathbf{4.21 \times 10^{-10}}$

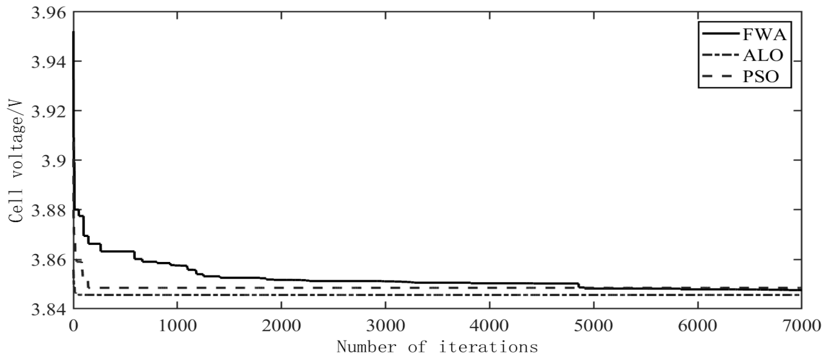

Figure 2. Convergence process curve.

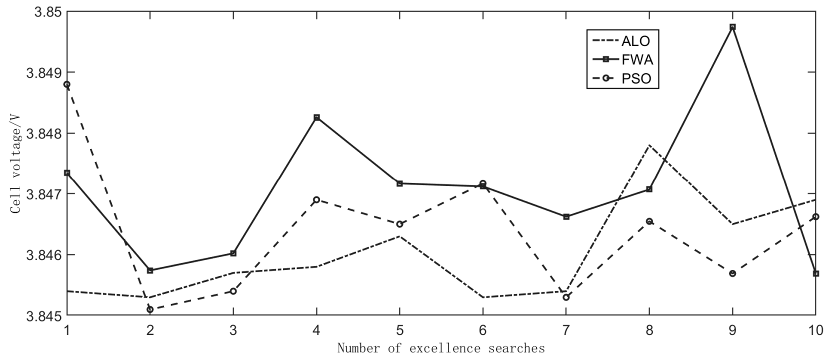

Figure 3. Cell voltage curve.

Table 7. Different algorithms standard deviation and mean.

	ALO	FWA	PSO
Average value	3.8454	3.8668	3.8464
Standard deviation	7.31×10^{-4}	10.83×10^{-4}	11.24×10^{-4}

It can be seen from Table 6 that the ALO algorithm is slightly worse than PSO in the three benchmark functions of F2, F11, and F12, but still better than FWA. Both the mean value and standard deviation of other benchmark functions are better than the other two algorithms, indicating that the ALO algorithm not only has a better optimization performance, but also has good robustness under the public data set. Compared with Figure 2, Figure 3, and Table 7, it can be seen that the convergence speed, convergence accuracy, and performance of the ALO algorithm in the actual data of aluminum electrolysis are superior to the other two algorithms, which is suitable for practical engineering problems of this topic.

A continuous time series of 300 sets of d_k cell-state metrics was selected as the experimental sample. Prior to the experiment, the samples must be differenced multiple times to smooth out the non-stationary time series. The AIC criterion was first used to determine the model order, and the ARMA (2,3) model was obtained in the experiments, and then this determined model was used to predict the time series of the composite index of cell state d. In addition, the ALO algorithm was also applied to order the model, and the resulting model order is (33,9), which is then used to predict d_{k+1}. The prediction results of the two models developed above are shown in Figure 4.

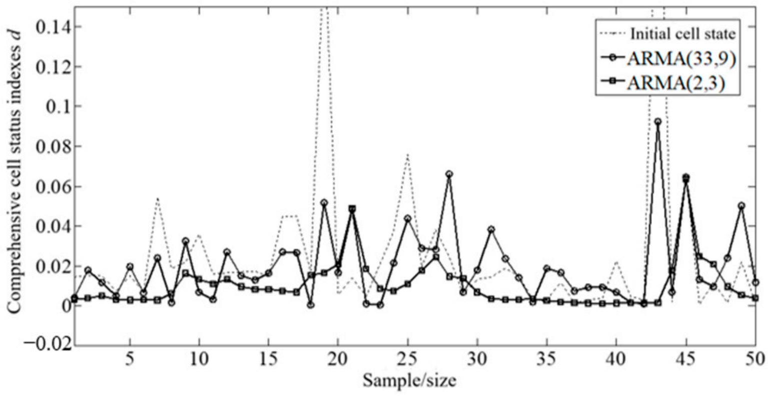

Figure 4. Time-series prediction of cell state index based on ALO-ARMA.

As shown in Figure 4, in general, both ARMA (2,3) and ARMA (33,9) can track the real time series, but the latter tracks better. To illustrate the tracking accuracy of the two models more accurately, the average prediction errors of the two models were calculated separately. As shown in Table 8, the tracking error of ARMA (2,3) is calculated to be 0.0139, while the tracking error of ARMA (33,9) is 0.0094, indicating that ARMA (33,9) has a higher tracking accuracy. The optimization of the order of ARMA using the ALO algorithm produces a set of optimal combinations of orders with the highest prediction accuracy, and the model has a higher accuracy than the model with the fixed order of the AIC criterion.

Table 8. Model prediction errors based on AIC and ALO.

Method of Ordering	Model	Prediction Error
AIC criterion	ARMA (2,3)	0.0139
ALO algorithm	ARMA (33,9)	0.0094

The composite indicators of cell state, d_{k+1} and x_4, x_5, x_6, and x_9 are used as inputs to the cell-state prediction model. After simply removing outliers, the processed 200 data sets were used as samples for the cell-state prediction experiments. Initially, 150 samples were selected as training data for the model and the remaining 50 data were used to test the trained model. The results of the cell-state prediction model are shown in Figure 5. As can be seen from the figure, 41 out of 50 samples are correctly predicted, with a prediction accuracy of 82%, indicating that the prediction model achieves a high level of accuracy and can be used as a reference for decision-makers in factories.

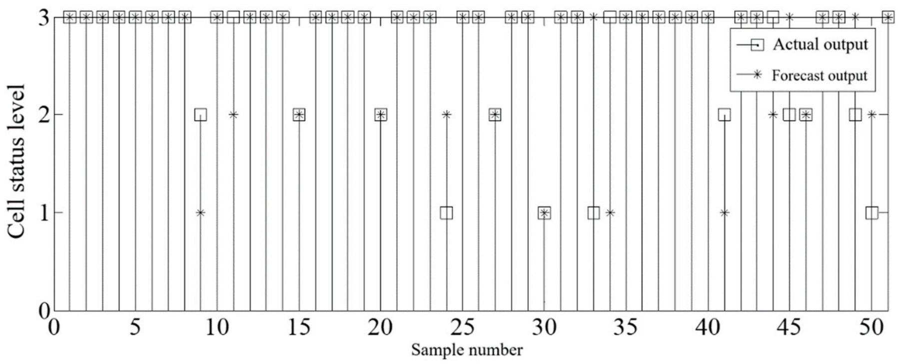

Figure 5. Training and testing results of cell-state prediction model based on FNN.

5.3. Optimization Setup Model Results

As described in Section 5.2 of this chapter, to obtain a set of optimized operating parameters, this experiment will solve the optimization setup model for 300 sets of historical data. A set of optimized operating parameters were found as follows. x_4 = 32.0557, x_5 = 3.9611, x_6 = 2.2464, and x_9 = 0.0118. Substituting this set of operating parameters into the cell-state prediction model, the prediction results show how the cell state changes when the electrolytic cell is set to this set of optimized parameters as shown in Figure 6. For example, at the ninth test point in Figure 6, when there is no output from the optimization setpoint, the state indicator d is 0.035, and the state of the electrolytic cell has deviated from the excellent state. This suggests that the optimization model can find an optimal set of operating parameters that will gradually bring a cell that has deviated from the optimum back to a good condition.

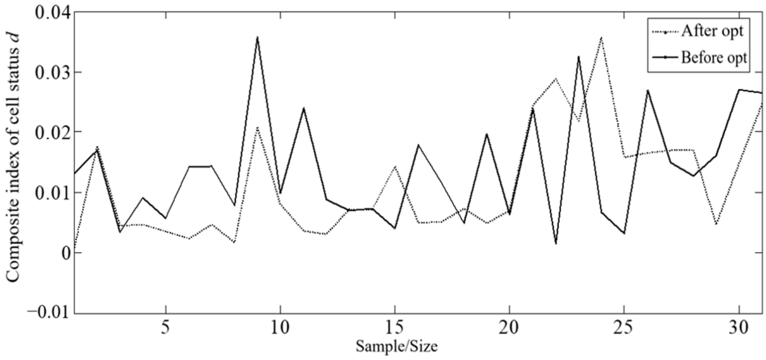

Figure 6. Cell state under optimal parameters.

Statistical information for the 31 state indicators d is shown in Table 9. The average value of the indicator d after optimization is 0.0026 lower than that before optimization, indicating that the cell condition is overall moving in the direction of excellence. The optimized variance is smaller, indicating that the cell state is gradually stabilized, and this set of optimized set values plays a role in stabilizing the cell state.

Table 9. Cell state index d before and after optimization.

d	Before Optimization	After Optimization
Average value	0.0140	0.0114
Variance	0.0092	0.0089

6. Conclusions

In this paper, a multi-objective optimization method for aluminum electrolysis process is proposed with the starting point of energy-saving and consumption-reducing production of aluminum electrolysis. To represent the three states of heat balance, material balance, and stability of the electrolytic cell, a comprehensive cell state index is defined, and the FCM is applied to judge the current cell state. In addition, a predictive model of the cell state was developed to predict the state after 24 h. Finally, the multi-objective optimal control of the aluminum electrolysis process is realized by establishing an optimization setting model. The method proposed in this paper focuses on the energy-saving and consumption-reducing production of aluminum electrolysis by setting operating parameters in case the cell condition develops into a bad cell. For the case of an excellent cell condition, the plant operator can realize energy-saving production of aluminum electrolysis by appropriately reducing the cell voltage without adjusting the electrolytic cell. When the cell condition develops into a vicious cell, the operating parameter optimization model can provide a set of reasonable operating parameter setting values. Then, the downstream control system can quickly stabilize the electrolytic cell and achieve energy saving and consumption reduction in the aluminum electrolysis production process through low-voltage production.

The above can provide a referable method for the aluminum electrolysis industry to achieve energy savings. However, since there may be more factors affecting the electrolytic cell with more uncertainties in an actual aluminum plant, the aluminum electrolysis production process should be analyzed from more perspectives in the future, such as such as cell condition diagnosis and superheat analysis of aluminum melting furnaces, in order to achieve a more energy-saving and higher energy-consumption reduction concept.

Author Contributions: Conceptualization, J.X.; Methodology, C.X.; Software, C.X.; Formal analysis, W.Z., D.L. and G.L.; Resources, J.C.; Data curation, W.Z.; Writing—original draft, C.X. and W.Z.; Writing—review & editing, C.X. and W.Z.; Funding acquisition, C.X. All authors have read and agreed to the published version of the manuscript.

Funding: This work was supported in part by the National Natural Science Foundation of China under Grant 62073090, and the Guangdong Polytechnic Normal University School Level Scientific Research Project No. 2021SDKYA118.

Data Availability Statement: The data presented in this study are not available due to privacy.

Conflicts of Interest: The authors declare no conflict of interest.

References

1. Liu, F.Q.; Qiu, D.S.; Gu, S.Q. Analysis on the Competitiveness and Development Trend of China's Aluminum Smelting Industry. *J. Eng. Sci.* **2022**, *44*, 561–572.
2. Yue, D.M.; Xu, W.; Wang, G.B.; Lin, H. Research on the current situation and development of Ningxia aluminum industry. *Light Metals* **2021**, 1–5. [CrossRef]
3. Zhou, Y.F.; Luo, L.F.; Wang, Y.F.; Li, C.L.; Zhang, F.F.; Zhang, F.P. Analysis and calculation of greenhouse gas emission reduction potential in aluminum electrolysis production process. *Light Metals* **2021**, 17–21. [CrossRef]
4. Zeng, Z.; Gui, W.; Chen, X.; Xie, Y.; Zhang, H.; Sun, Y. A cell condition-sensitive frequency segmentation method based on the sub-band instantaneous energy spectrum of aluminum electrolysis cell voltage. *Engineering* **2021**, *7*, 1282–1292. [CrossRef]
5. Xu, C.H.; Wu, G.H. Cell Voltage Optimization Method Based on STA-LSSVM. *Meas. Control Technol.* **2023**, *42*, 110–118.
6. Xu, C.H.; Tu, Z.C.; Zhang, W.J.; Cen, J.; Xiong, J.; Wang, N. A Method of Optimizing Cell Voltage Based on STA-LSSVM Model. *Mathematics* **2022**, *10*, 4710. [CrossRef]
7. Cui, G.M.; Yang, H.J.; Liu, P.L.; Yu, K. Prediction of Alumina Density in Aluminum Electrolysis Based on Data. *Comput. Simul.* **2018**, *35*, 305–309.
8. He, W. Research on prediction method of anode effect of aluminum electrolytic cell based on deep learning. *China Nonferrous Metall.* **2022**, *51*, 112–117.
9. Gao, T.; Zhang, K.; Shi, H.; Zhao, J.; Li, J. A two-stage classifier switchable aluminum electrolysis fault diagnosis method. *Trans. Inst. Meas. Control.* **2022**, *44*, 1708–1720. [CrossRef]
10. Hou, J.; Tian, X.F.; Kong, S.Q. Prediction of aluminum pot conditions based on LSTM. *Light Met.* **2021**, 33–37+62.
11. Xu, C.H.; Ping, J.M.; Lin, X.F.; Huang, Q.B.; Li, Z. Optimization Method of the Cell Voltage Based on The Improved Multiple Extreme Learning Machine. *Control. Eng. China* **2020**, *27*, 758–764.
12. Li, Z.Y.; Yang, S.; Zou, Z.; Li, J. Research progress of on-line detection for spatial distribution information in large-amperage aluminum reduction cells. *Light Met.* **2019**, *9*, 22–30.
13. Fan, Q.; Long, W.; Yao, L.Z.; Li, Y.Y. Multi-objective optimization of aluminum electrolysis based on functional evolution operator. *J. Sichuan Univ.* **2021**, *58*, 90–98.
14. Lin, M.; Ma, L. Research on Setting Voltage of Electrolyzer Based on LGBM-LSTM Algorithm. In Proceedings of the 2021 IEEE 4th International Conference on Computer and Communication Engineering Technology (CCET), Beijing, China, 13–15 August 2021; pp. 414–419.
15. Xu, C.; Zhang, J.; Cheng, R.; Chen, R.; Luo, Z.-G.; Li, H.-R. A ALO-LSSVM Model for the Cell Voltage Optimization in Aluminum Electrolysis Process. In Proceedings of the 2020 39th Chinese Control Conference (CCC), Shenyang, China, 27–29 July 2020; pp. 1431–1436.
16. Zhou, J.; Chen, X.; Xie, S.; Xie, Y. Anode Current for Aluminum Electrolysis Cell Condition Identification Based on Improved Temporal Convolutional Network. In Proceedings of the 2021 6th International Conference on Robotics and Automation Engineering (ICRAE), Guangzhou, China, 19–22 November 2021; pp. 35–39.
17. Lundby, E.T.B.; Rasheed, A.; Gravdahl, J.T.; Halvorsen, I.J. A novel hybrid analysis and modeling approach applied to aluminum electrolysis process. *J. Process Control.* **2021**, *105*, 62–77. [CrossRef]
18. Shuang, L.; Yong, B.L.; Zhong, Y.Z. Multi-index Evaluation Modeling Method Based on AHP and PCA and Its Application. *Inf. Control.* **2015**, *44*, 416–421.
19. Peng, H.; Zhang, S.; Li, L.; Qu, B.; Yue, X.; Wu, Z. Multi-strategy multi-modal multi-objective evolutionary algorithm using macro and micro archive sets. *Inf. Sci.* **2024**, *663*, 120301. [CrossRef]
20. Song, M. Visual Analysis of Project Investment Decision Information Platform based on FCM Algorithm. In Proceedings of the 2023 International Conference on Inventive Computation Technologies (ICICT), Lalitpur, Nepal, 26–28 April 2023.

21. Feng, Z.; Ding, W.; Cao, J.; Sun, C.; Shen, X.; Wang, H. Adaptive FCM Clustering Algorithm Based on Twin Multiple Population Genetic Evolution. In Proceedings of the 2021 IEEE 1st International Conference on Digital Twins and Parallel Intelligence (DTPI), Online, 15 July–15 August 2021.
22. Gao, Z.; Chen, Y.; Li, Z.; Li, T.; He, J.; Li, Y. An Improved Crowd Aggregation Prediction Algorithm Based on ARMA. In Proceedings of the 2022 6th International Conference on Innovation in Artificial Intelligence, Guangzhou, China, 4–6 March 2022.
23. Sansa, I.; Boussaada, Z.; Mrabet Bellaa, N. Solar radiation prediction using a novel hybrid model of ARMA and NARX. *Energies* **2021**, *14*, 6920. [CrossRef]
24. Wang, H.; Chen, Y.; Yu, H.; Xi, J. Social Cascade FNN: An Interpretable Learning-Based Decision-Making Framework for Autonomous Driving in Lane Changing Scenarios. In Proceedings of the 2023 IEEE 26th International Conference on Intelligent Transportation Systems (ITSC), Bizkaia, Spain, 24–28 September 2023.
25. Guo, J.; Gui, W.H.; Wen, X.H. Multi-objective optimization for aluminum electrolysis production process. *J. Cent. South Univ.* **2012**, *43*, 548–553.
26. Lotfan, S.; Fathi, R. Parametric modeling of carbon nanotubes and estimating nonlocal constant using simulated vibration signals-ARMA and ANN based approach. *J. Cent. South Univ.* **2018**, *25*, 461–472. [CrossRef]
27. Sharma, D.; Lie, T.T.; Nair, N.K.C.; Vallès, B. Wind speed forecasting using ANN, ARMA and AIC hybrid to ensure power grid reliability. In Proceedings of the 2015 IEEE Innovative Smart Grid Technologies-Asia (ISGT ASIA), Bangkok, Thailand, 3–6 November 2015; pp. 1–5.
28. Tang, W.H.; Röllin, A. Model identification for ARMA time series through convolutional neural networks. *Decis. Support Syst.* **2021**, *146*, 113544. [CrossRef]
29. Lv, W.; Zhu, X. Prediction of complaints at civil aviation airports based on ARMA model. In Proceedings of the Fourth International Conference on Computer Science and Communication Technology (ICCSCT 2023), Wuhan, China, 26–28 July 2023; Volume 12918, pp. 134–140.
30. Mirjalili, S. The ant lion optimizer. *Adv. Eng. Softw.* **2015**, *83*, 80–98. [CrossRef]
31. Nagabushanam, D.S.; Mathew, S.; Chowdhary, C.L. A study on the deviations in performance of FNNs and CNNs in the realm of grayscale adversarial images. *arXiv* **2022**, arXiv:2209.08262.
32. Zhu, J.; Hu, X.; Lou, Y. Ultra short term wind power forecasting method based on projection pursuit algorithm. In Proceedings of the 3rd International Conference on Applied Mathematics, Modelling, and Intelligent Computing (CAMMIC 2023), Tangshan, China, 24–26 March 2023; Volume 12756, pp. 559–563.
33. Koziel, S.; Pietrenko-Dabrowska, A. Constrained multi-objective optimization of compact microwave circuits by design triangulation and pareto front interpolation. *Eur. J. Oper. Res.* **2022**, *299*, 302–312. [CrossRef]
34. Gilani, V.N.M.; Hosseinian, S.M.; Behbahani, H.; Hamedi, G.H. Prediction and pareto-based multi-objective optimization of moisture and fatigue damages of asphalt mixtures modified with nano hydrated lime. *Constr. Build. Mater.* **2020**, *261*, 120509. [CrossRef]
35. Xu, C.; Zhang, W.; Tu, Z.; Liu, D.; Cen, J.; Song, H. Improved moth-flame algorithm based on cat chaotic and dynamic cosine factor. *Rev. Sci. Instrum.* **2024**, *95*, 024703. [CrossRef] [PubMed]